

# Properties of M31. V: 298 Eclipsing Binaries from PAndromeda

C.-H. Lee<sup>1,2</sup>, J. Koppenhoefer<sup>2,1</sup>, S. Seitz<sup>1,2</sup>, R. Bender<sup>1,2</sup>, A. Riffeser<sup>1,2</sup>, M. Kodric<sup>1,2</sup>, U. Hopp<sup>1,2</sup>, J. Snigula<sup>2,1</sup>, C. Gössl<sup>1,2</sup>, R.-P. Kudritzki<sup>3</sup>, W. Burgett<sup>3</sup>, K. Chambers<sup>3</sup>, K. Hodapp<sup>3</sup>, N. Kaiser<sup>3</sup>, C. Waters<sup>3</sup>

## ABSTRACT

The goal of this work is to conduct a photometric study of eclipsing binaries in M31. We apply a modified box-fitting algorithm to search for eclipsing binary candidates and determine their period. We classify these candidates into detached, semi-detached, and contact systems using the Fourier decomposition method. We cross-match the position of our detached candidates with the photometry from Local Group Survey (Massey et al. 2006) and select 13 candidates brighter than 20.5 magnitude in V. The relative physical parameters of these detached candidates are further characterized with Detached Eclipsing Binary Light curve fitter (DEBiL) by Devor (2005). We will follow-up the detached eclipsing binaries spectroscopically and determine the distance to M31.

*Subject headings:* Binaries: eclipsing – stars: distances – stars: fundamental parameters – galaxies: individual (M31)

## 1. Introduction

Eclipsing binaries are important in two aspects. First of all, they can provide information on the physical parameters of the system. For example, their light-curves can be used to derive the inclination angle of their orbital plane, and the stellar radius in terms of the orbital distance. The spectroscopic observation can be used to infer the mass of individual stars, the orbital distance, and stellar temperature. These information are essential for the theoretical study of stellar evolution.

Secondly, eclipsing binaries can serve as distance indicators. This is possible because once we know the stellar radius and temperature from joint photometric and spectroscopic observations, we can derive the distance ( $d$ ) by:

$$f_{\lambda} = \frac{1}{d^2} (R_1^2 F_{1,\lambda} + R_2^2 F_{2,\lambda}) \times 10^{-0.4A(\lambda)}, \quad (1)$$

---

<sup>1</sup>University Observatory Munich, Scheinerstrasse 1, 81679 Munich, Germany

<sup>2</sup>Max Planck Institute for Extraterrestrial Physics, Giessenbachstrasse, 85748 Garching, Germany

<sup>3</sup>Institute for Astronomy, University of Hawaii at Manoa, Honolulu, HI 96822, USA

where  $R_{1,2}$  are the radii of the primary and secondary,  $F_{1,\lambda}$  and  $F_{2,\lambda}$  are the surface fluxes of the primary and secondary components, and  $A(\lambda)$  is the total extinction:

$$A(\lambda) = E(B - V)[k(\lambda - V) + R_v], \quad (2)$$

where  $E(B - V)$  is the reddening,  $k(\lambda - V)$  is the normalized extinction curve defined as  $E(\lambda - V)/E(B - V)$ , and  $R_v$  is the ratio of total to selective extinction in V band. By matching the model atmospheres to the broad band photometry, we are able to determine the value of  $E(B - V)$  and  $R_v$  and estimate the extinction, which is usually hard to measure and assumed  $R_v=3.1$ .

It is worth to note that according to the extent of Roche-lobe filling and the deformation of the stellar surface, eclipsing binaries can be classified into subclass of detached, semi-detached and over-contact. It has been suggested that the detached eclipsing binaries are more suitable for distance determination (see e.g. Paczyński 1997), although some authors argue that the Roche-lobe filling semi-detached eclipsing binaries can put more constraints on the light-curve modeling thus have advantages to be standard candle as well (Wyithe & Wilson 2002).

Previous studies of extra-galactic distance determination used the Large Magellanic Cloud (LMC) as a distance anchor. While LMC bears irregularity in its three dimensional shape and low metallicity, many authors suggest to use M31 as a stepping stone to the cosmic distance determination (see e.g., Clementini et al. 2001; Vilardell et al. 2010, and reference therein). The merits of M31 include its simple geometry, the stars that are potential distance indicators in M31 are bright enough to be resolved, a local counter-part of the spiral galaxies that are used to determine the extra-galactic distance (see e.g., Freedman et al. 2001), and a local benchmark to calibrate the Tully-Fisher relation.

In order to detect the eclipsing binaries in M31, one requires to monitor a large fraction of M31 with high cadence. Previous studies, e.g. the *DIRECT* project (Kaluzny et al. 1998; Stanek et al. 1998, 1999; Kaluzny et al. 1999; Mochejska et al. 1999; Bonanos et al. 2003) observed M31 with a  $11' \times 11'$  field of view (FOV) in 1996 and 1997, and later expanded to a  $22' \times 22'$  FOV in 1998 and 1999, in a mosaic way to cover an area of  $0.5 \text{ degree}^2$  (Macri 2004). On the other hand, Vilardell et al. (2006) use the  $33.8' \times 33.8'$  Wide Field Camera on-board the Isaac Newton Telescope in Spain to observe the north-eastern part of M31 from 1999 to 2003 (in total 21 nights). The limitations of these studies is that their observations only cover part of M31 disk. With the  $\approx 7 \text{ degree}^2$  FOV of Pan-STARRS 1 (PS1), we are able to cover the entire disk of M31 in one shot (see e.g. Fig. 1 of Lee et al. 2013) with a time resolution of up to 0.5 day. The PS1 started to observe M31 since 2010. Here we present the results from the three year PS1 monitoring.

This paper is organized as follows. In section 2 we present our data analysis. In section 3 we describe our procedure to search for periodic variable sources, and invented a modified box-fitting method to identify eclipsing binary candidates. Classifications of our binary candidates are presented in section 4. We cross-match detached binaries in our sample with the Local Group Survey to find binaries that are ideal to follow-up; we further use the Detached Eclipsing Binary

Light curve fitter to characterize these bright candidates, and extract their parameters in section 5, followed by a summary in section 6.

## 2. Data Analysis

The Pan-STARRS 1 (hereafter PS1) survey<sup>1</sup> uses a 1.8 meter telescope equipped with a gigapixel camera (GPC) located at Haleakala in Hawaii. The camera consists of 60 detectors, each detector is segmented in an  $8 \times 8$  array of  $590 \times 598$  pixel cells. Each pixel has a size of  $10 \mu\text{m}$ , corresponding to  $0.258''/\text{pixel}$ . The FOV of each detector is  $20'.95 \times 20'.74$  and the FOV of the 60 detectors is approximately  $7 \text{ degree}^2$ .

The PS1 survey includes dedicated observations of M31, the so-called PAndromeda project. PAndromeda makes use of  $\sim 2\%$  of the PS1 observation time, starting from July until December each year, to monitor M31. In this work we present the result of the three-year PAndromeda data, taken between 2010 and 2012. The original design of PAndromeda is to search for short timescale microlensing events, thus we monitor M31 in two time block per night, separated by three to five hours, to have a time resolution of less than one day. Such high-cadence observation strategy is also useful for short period variables. The two observation blocks yield 12 observations in  $r_{P1}$  and 6 observations in  $i_{P1}$ , with an exposure time of 60 seconds. The observations in each block are combined to increase the S/N. In the end we have 330 epochs in  $r_{P1}$  and 250 epochs in  $i_{P1}$ .

After the images are taken with the PS1 telescope, they are processed by the Image Processing Pipeline (IPP, Magnier 2006). The pipeline runs several successive steps, including bias and dark correction, masking, artifact removing, flat-fielding, astrometric calibration (Magnier et al. 2008), and resampling to a common pixel scale to a sky-based image plane, so-called skycells.

Afterwards, we perform Difference Imaging Analysis (DIA, Alard & Lupton 1998) using our customized software MDia (Koppenhoefer et al. 2013) and generate light-curves of all point sources. Details of our analysis can be found in Lee et al. (2012) and Kodric et al. (2013).

## 3. Search for Variability

In order to identify all periodic signals that can be attributed to eclipsing binaries systems we apply a detection algorithm to all 738,755  $r_{P1}$ -band light curves that have been extracted from the PAndromeda data. Our detection procedure is based on the boxfitting algorithm (Kovács et al. 2002) which has been developed to detect box-shaped brightness decreases such as planetary transits. We run the boxfitting algorithm using 100001 test periods between 0.25 days and 19.1 days which are equally distributed in  $1/p$ . The duration of the eclipses is limited to 0.25 phase units.

---

<sup>1</sup><http://pan-starrs.ifa.hawaii.edu/public/>

The algorithm is known to be also useful to detect detached and semi-detached eclipsing binary systems (e.g. Nefs et al. 2012), however, due to the larger ratio between the radii of the primary and secondary star the light curves of eclipsing binaries are generally more V-shaped than in the case of planetary transits. In order to account for that we refit the folded light curve for each detected period with a symmetric trapezium that has the same full width half maximum as the best fitting box. The approach has been used by Zendejas Dominguez et al. (2013) already. We define the V-shape parameter as the fraction of the time spend in ingress and egress with respect to the total duration of the eclipse:

$$V = (T_2 - T_1 + T_4 - T_3)/(T_4 - T_1), \quad (3)$$

with  $T_1$  and  $T_2$  being the phase values at the beginning and end of the ingress and  $T_3$  and  $T_4$  being the phase values at the beginning and end of the egress. Note that the values of  $T_1$ ,  $T_2$ ,  $T_3$ , and  $T_4$  are parameters that are fitted when applying the detection algorithm and they do not relate in a direct way to the really start/end of the ingress/egress of the light curve since the fitted trapezium model is only an approximation of the real brightness variation. With this definition,  $V = 0$  corresponds to a pure box-shaped eclipse and  $V = 1$  corresponding to an eclipse without flat central part (i.e.  $T_2 = T_3$ ). In addition we define the signal-to-noise ratio (S/N) of the detection as the eclipse depth  $\delta$  divided by the standard deviation  $\sigma_{ecl}$  of the combination of all points during the eclipse (i.e. all points between  $(T_1 + T_2) / 2$  and  $(T_3 + T_4) / 2$ ):

$$S/N = \frac{\delta}{\sigma_{ecl}}. \quad (4)$$

We calculate the S/N for both the primary and the secondary eclipse. After removing the eclipses we re-run the boxfitting algorithm a second time on each light curve and calculate the S/N of the best fitting period  $S/N_{removed}$ . This value is a good measure for the variation of the out-of-eclipse part of the candidate and can be used to distinguish eclipsing binaries from other variable sources (see below).

Eclipsing binary light curves usually show a secondary eclipse which is offset by 0.5 in phase units for circular orbits. We therefore fit a secondary eclipse for each period that has been detected by the boxfitting algorithm. The secondary eclipse is first fitted as a box which is offset by exactly 0.5 phase units from the center of the primary eclipse and subsequently refined to a trapezium shape in the same way the primary eclipse has been refined. Fig. 1 shows an example folded lightcurve of one of our detected eclipsing binaries together with the best fitting trapezium-shaped primary and secondary eclipse models.

Since the boxfitting algorithm searches only for one eclipse in the folded light curve the best fitting period for eclipsing binary light curves usually corresponds to half the true period with the primary and secondary transit folded together. The true binary period is found as the second or

third best fitting period. We therefore select the six best fitting periods for each input light curve and select the period with the lowest  $\chi^2$  of the refined fit that is including a secondary eclipse (see above).

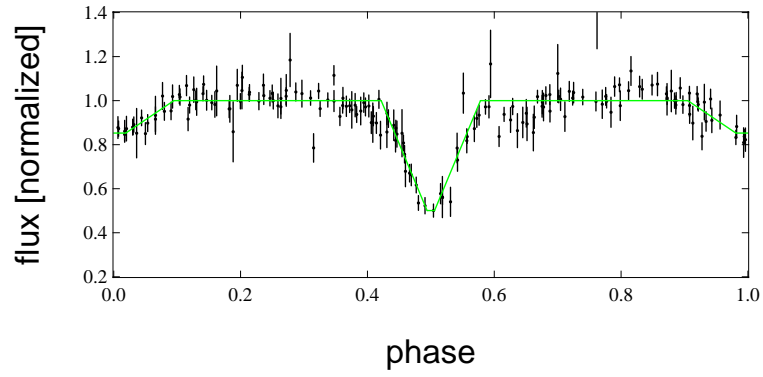


Fig. 1.— Example normalized and phase-folded light curve of one of the detached eclipsing binaries we detected in M31. The overplotted green line shows the best fitting trapezium model as fitted by our detection algorithm.

We apply a number of criteria to select the best eclipsing binary candidates. First we reject all detections with periods close to alias periods that are enhanced by the window functions of the observations. The alias periods are identified as peaks in the histogram of detected periods. In addition we require a candidate to have at least 10 points in the primary eclipse and 5 points in the secondary eclipse. We split the remaining detections in two samples:

- The high S/N sample contains all light curves with an *RMS* of the out-of-eclipse part of the light curve of lower than 0.20 and an effective signal-to-noise ratio  $S/N_{eff}$  larger than 12.  $S/N_{eff}$  is calculated as the sum of the S/N of primary and secondary eclipse reduced by  $S/N_{removed}$  (see above).
- The low  $\chi^2$  sample contains all light curves with a reduced  $\chi^2$  of the refined binary fit lower than 2 and a sum of the S/N of primary and secondary eclipse larger than 12.

We visually inspected 5344 candidates in the high S/N sample and 824 candidates in the low  $\chi^2$  sample and identified 298 eclipsing binary systems. The remaining candidates were false detections due to systematic outliers and pulsating variable stars such as  $\delta$ -Cepheids. Note that we only select light curves for which the primary and secondary eclipses show a symmetric shape in order to have a clean sample.

The number of 298 eclipsing binaries is a rather small value compared with Vilardell et al. (2006). The reason for the relatively low number of detected eclipsing binaries is due to the relatively short exposure times of the current work compared to Vilardell et al. (2006). Note also that we only select eclipsing binary systems with high signal to noise ratio and good light curves.

#### 4. Classification

In this section we attempt to classify our eclipsing binaries based on the shape of their light curves. The broadly used taxonomy of eclipsing systems is based on the resemblance of light curves to certain prototypes, which are categorized in Algol-type (EA),  $\beta$  Lyrae-type (EB), and W Ursae-Majoris-type (EW), see e.g. General Catalog of Variable Stars (GCVS database Samus et al. 2009). However, this classification scheme does not fully reflect the physical configuration of a binary system. Alternatively, we classify our binary systems based on the scheme of detached (ED), semi-detached (ESD), and contact (EC), which reflect the Roche-lobe filling status of both components.

Following the procedure of Rucinski (1993) and Pojmanski (2002), we classify our candidates with the Fourier decomposition method by fitting the phase-folded normalized light curves with a

series of sine and cosine functions:

$$f(\phi) = \sum_{i=1}^4 a_i \cos(2\pi i \phi) + b_i \sin(2\pi i \phi) \quad (5)$$

where  $f(\phi)$  is the normalized flux at phase  $\phi$ . It has been shown the different configurations of eclipsing binaries are separated on the  $a_2$ - $a_4$  plane. Such approach has been used to classify eclipsing binaries in the Milky Way from the ASAS sample (Pojmanski 2002) and in the Magellanic Clouds from the MACHO sample (Derekas et al. 2007). Before extending this classification scheme to our sample, we verify this classification scheme using two well-studied binaries in M31 (Ribas et al. 2005; Vilardell et al. 2010), where their configurations are well-known from joint analysis of photometric and spectroscopic analysis. The fourier decomposition method returns the correct configuration for these two extra-galactic binaries. We thus adopted the boundary values of  $a_2$  and  $a_4$  from Pojmanski (2002) and classify our candidates accordingly. The results can be seen in Fig. 3. To have an idea of how robust the  $a_2$  and  $a_4$  parameters are determined from the light curves, we perform a bootstrapping test on each light curve for 100 iterations, and calculate the standard deviation within these 100 iterations. The standard deviation of  $a_2$  and  $a_4$  is then plotted as error-bar in Fig. 3.

We note that there are fewer contact binaries (22) than detached (120) and semi-detached (158) systems, in contrary to the results of Milky Way sample from the All Sky Automated Survey (ASAS) in Paczyński et al. (2006). This might be contributed by the combination of intrinsic faintness of the contact system and the remoteness of M31. The expected brightness of contact binaries in M31 can be derived using the period-luminosity relation from Rucinski (1996):

$$M_V = -2.38 \log P + 4.26(B - V) + 0.28 \quad (6)$$

with an  $1-\sigma$  dispersion of 0.24. Assuming a period of 1 day, a (B-V) color of 0.0 (see Fig. 2), and given a distance modulus of 24.36 mag for M31 (Vilardell et al. 2010), the period-luminosity relation predicts a observed magnitude of  $V=24.12$  mag, which is not reached in the PAndromeda survey. Hence, our contact binary candidates are either more likely to reside in the foreground, or indeed belong to M31 but have longer periods. In addition, our search algorithm limits the duration of the eclipses to be 0.25 in orbital phase; while contact binaries have largely sinusoidal light curves and the eclipses can span more than half of the orbital phase, the highly distorted contact systems can be missed by our algorithm, hence the detection bias can affect the number of the contact systems as well.

The spatial distribution of our binary candidates are shown in Fig. 4. From the spatial distribution, there are some binaries located outside the main disk of M31, which could be attributed to foreground stars in the Milky Way. Indeed, one of our bright detached system presented in section 5, i.e. 036-15741, falls outside the main disk of M31, and is too bright/red to fit into the M31 scenario, hence we attribute it to be a foreground Milky Way system. From the ASAS Milky Way sample, the detached systems are concentrated on the Galactic plane, suggesting that



these are more massive and intrinsic brighter systems, while the contact systems are isotropically distributed (Paczynski et al. 2006). However, due to our limited sample of contact binaries and the highly inclined disk of M31, we could not distinguish the difference in spatial distribution of these two different systems. In addition, we would like to note that the eclipsing binaries detected in the survey will likely have rather bright and blue components (see e.g. Fig. 4 in Vilardell et al. 2006) and are expected to have young massive components, hence mostly distributed along the spiral arms. To verify this hypothesis, we cross-matched our eclipsing binaries with the photometry of Massey et al. (2006) to derive their colors and present their color-magnitude diagram in Fig. 2, and find out that they indeed exhibit blue colors.

We also show the period distribution in Fig. 5. The contact systems dominate the short period range, while the detached and semi-detached systems are peaked at  $\log P > 1$  day, in agreement with the results of Milky Way sample from ASAS. The only exception is a contact system with period larger than 10 days. We check the error budget of  $a_2$  and  $a_4$  estimated from bootstrapping, which indicates a solid contact classification on the  $a_2$ - $a_4$  plane. We note that there are several apparently contact systems with period larger than 10 days reported by Rucinski & Maceroni (2001). Such systems can be explained by a semi-detached scheme, where one of the component is filling its Roche lobe and the other component is small or with lower temperature, thus the light curve reflects only the ellipsoidal variations of the larger, Roche-filling component. The color of such systems is red compared to normal contact systems. We thus cross-match the position with the local group survey (Massey et al. 2006), and found that the color of our long-period contact binary is indeed red, with  $(V-I) = 0.824$ , and belongs to the long-period semi-detached scheme as shown in Fig. 2 of Rucinski & Maceroni (2001).

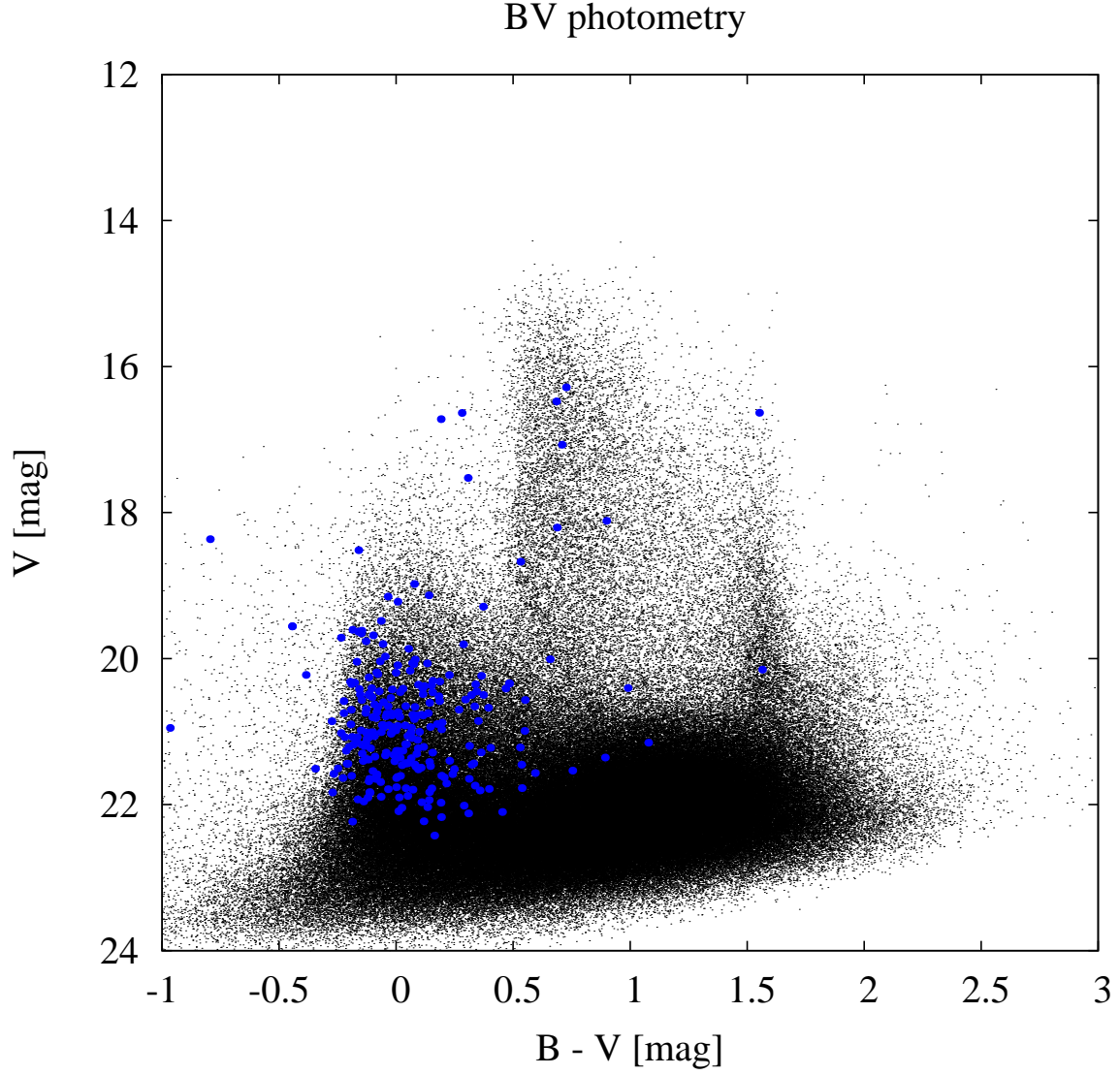


Fig. 2.— Color magnitude diagram for the detected eclipsing binaries. The underlying black dots are photometric measurements taken from the Local Group Galaxy Survey (Massey et al. 2006). The detected eclipsing binaries exhibit blue colors, allude to young, massive components that populate the spiral arms.

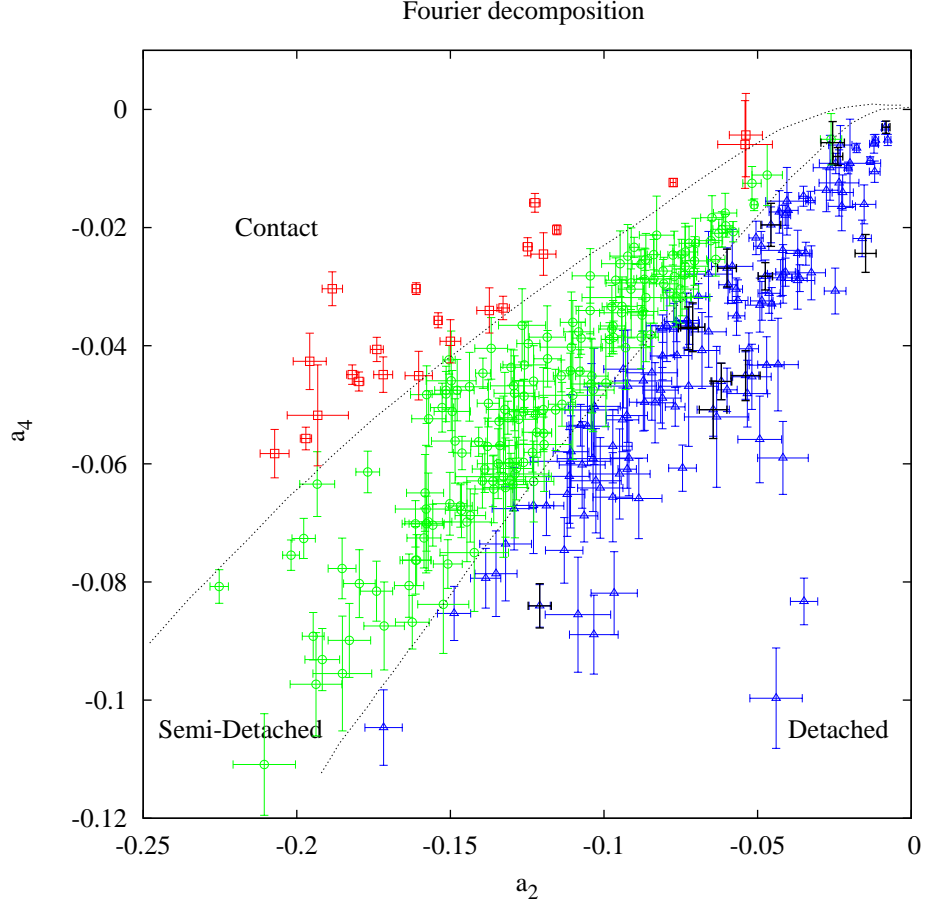


Fig. 3.— Classifying binary candidates using the Fourier decomposition parameters  $a_2$  and  $a_4$  in equation 5. Blue triangles denote the detached systems, green circles indicate the semi-detached systems, while red squares represent the contact systems. The black error bars indicate the bright detached systems discussed in section 5. The two dotted curves delineate the boundaries of different systems, as shown in Pojmanski (2002).

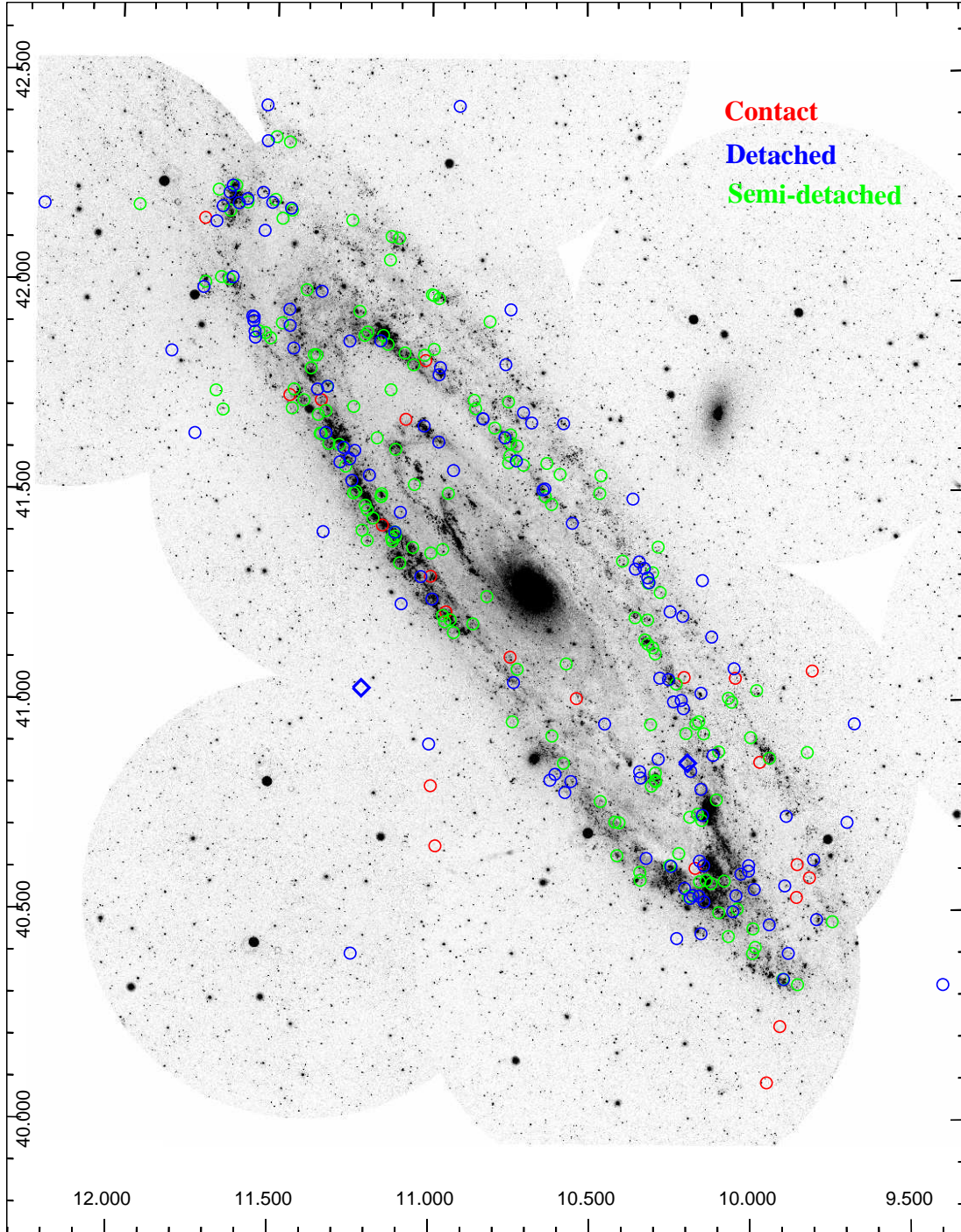


Fig. 4.— Spatial distribution of different binary configurations. Contact systems are marked in red, semi-detached systems are marked in green, and the detached systems are marked in blue. Please note that the two foreground detached systems discussed in section 5 are marked in rhombi. The underlying image is taken from GALEX (Gil de Paz et al. 2007).

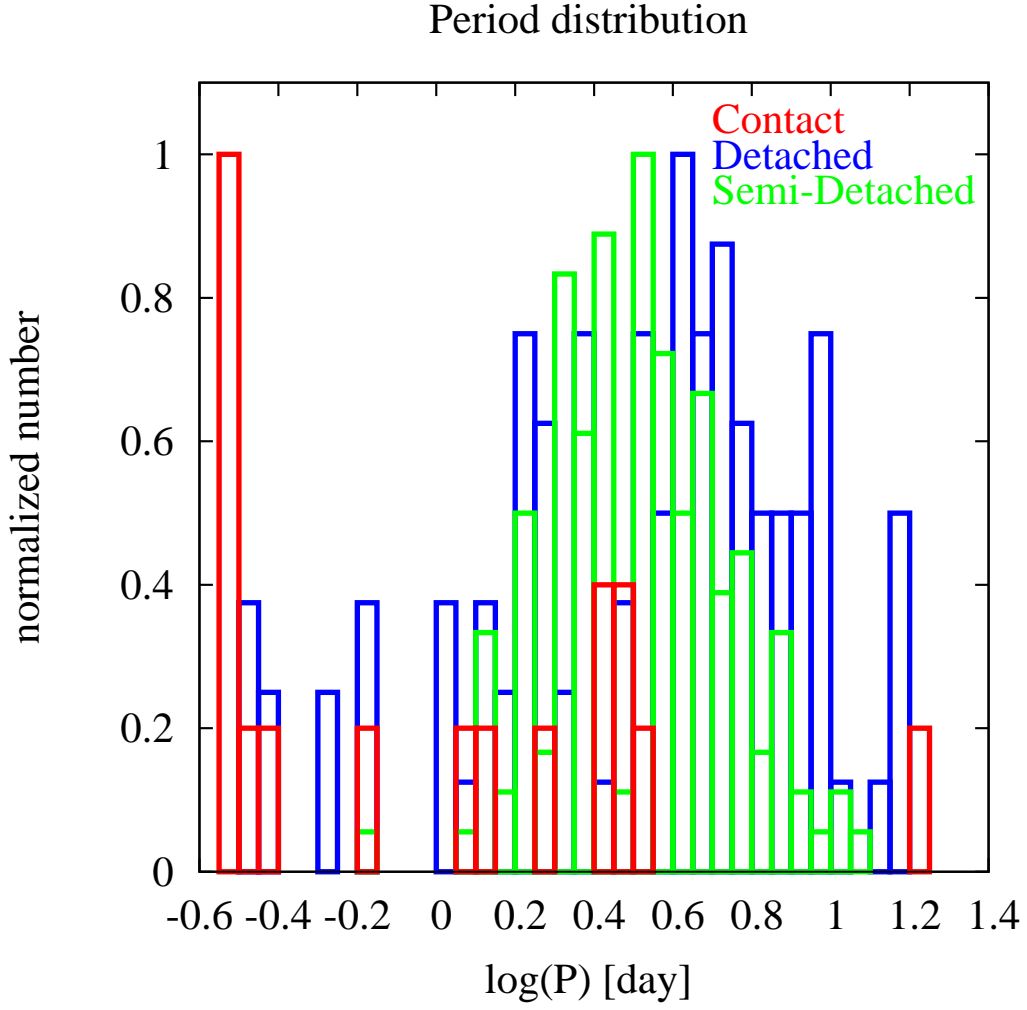


Fig. 5.— Period distribution of different binary configurations. Contact systems are shown in red, detached systems are marked in blue, and the semi-detached systems are denoted in green. Most of the contact systems show relatively short periods, while the detached and semi-detached systems are peaked at period larger than 1 day.

## 5. Detached binaries suitable for distance determination

We cross-match our detached binaries with the catalog of Local Group Survey (Massey et al. 2006), and among the 298 binaries in our sample we find 13 candidates brighter than 20.5 mag in V, for which we could obtain radial velocity information from 8-10 m class telescopes in a reasonable amount of time. We further fit their light curves with the Detached Eclipsing Binary Light curve fitter (DEBiL) developed by Devor (2005). Provided with an eclipsing binary light curve and its period, DEBiL can determine the eccentricity ( $e$ ), the radius of the primary and secondary component in units of semi-major axis ( $R_1/a$  and  $R_2/a$ ), and the inclination angle ( $\sin i$ ) of the binary system in a robust manner. The results of the best-fitted model are shown in Table 1. Please note that the eccentricity is always fitted, but we only show the ones with errors smaller than the value of  $e$ . For the cases where the errors are larger than  $e$ , we consider the eccentricity as insignificant and show the best-fit value plus the error as an upper limit in Table 1. Note that in such cases, it can be either that there is negligible eccentricity, or that the semi-major axis is aligned to our line-of-sight, hence the eccentricity effect on the light curve is compromised. DEBiL can only give symmetric errors, which are shown in Table 1 following the best-fitted values of each parameter. The light curves, as well as the best-fitted DEBiL models, are shown in Fig. 6

Among the 13 bright detached binary systems, we find two of them are too bright to fit into M31 scenario, hence could be foreground stars. To assess their origin as Milky Way foreground stars, we investigate the color magnitude diagram using B-V v.s. V, where the M31 blue super giants, the foreground dwarves and giants from Milky Way are clearly separated, as shown in Massey et al. (2006). We find that the two brightest systems, 034-19151 and 036-15741 exhibit relatively red color and fit into the Milky Way foreground dwarf scenario, while the remaining 11 systems are bluer and better fit into the M31 blue giants scenario, as shown in Fig. 7.



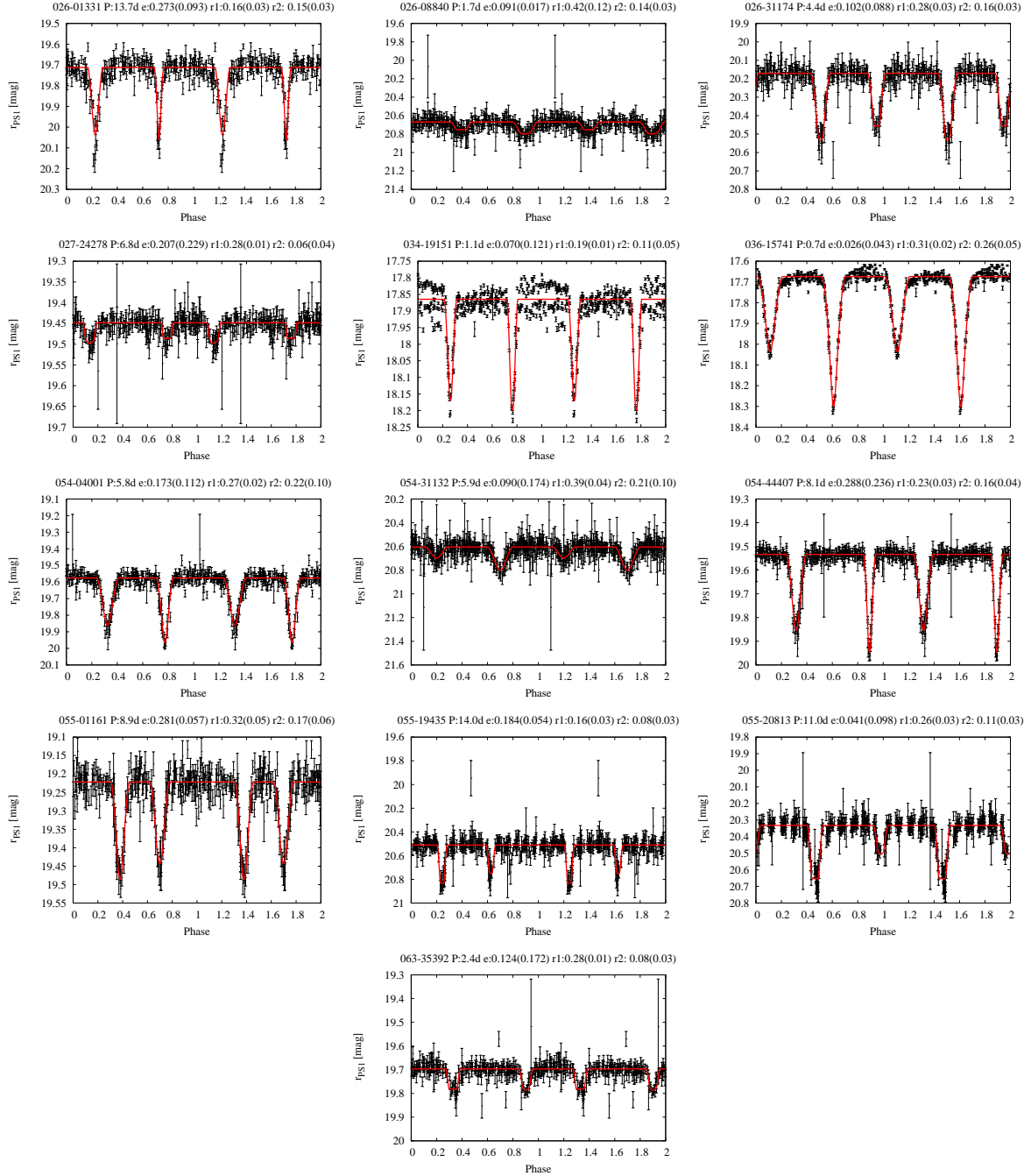


Fig. 6.— Lightcurves and best-fitted DEBiL model for the 13 detached binaries. The parameters in top of each panel are explained in Table 1, see also text.

Table 1: Best-fit DEBiL model of bright detached binary systems.

Name	RA(J2000) [deg]	Dec(J2000) [deg]	Period [day]	$e$	$R_1/a$	$R_2/a$	$\sin(i)$	V [mag]	B-V [mag]
026-01331	9.8894899	40.3386213	13.7	$0.27 \pm 0.09$	$0.16 \pm 0.03$	$0.15 \pm 0.03$	$0.99 \pm 0.01$	19.151	-0.036
026-08840	10.1470368	40.4485614	1.7	$0.09 \pm 0.02$	$0.42 \pm 0.12$	$0.14 \pm 0.03$	$0.99 \pm 0.34$	20.484	-0.116
026-31174	10.1376832	40.6107178	4.4	$0.10 \pm 0.09$	$0.28 \pm 0.03$	$0.16 \pm 0.03$	$1.00 \pm 0.02$	20.042	-0.169
027-24278	9.7924434	40.6230922	6.8	$\leq 0.44$	$0.28 \pm 0.01$	$0.06 \pm 0.04$	$0.99 \pm 0.07$	20.061	0.068
034-19151	11.2190806	41.0353092	1.1	$\leq 0.19$	$0.19 \pm 0.01$	$0.11 \pm 0.05$	$1.00 \pm 0.01$	18.113	0.898
036-15741	10.1831493	40.8530845	0.7	$\leq 0.07$	$0.31 \pm 0.02$	$0.26 \pm 0.05$	$0.99 \pm 0.01$	18.204	0.687
054-04001	11.0970184	41.4524026	5.8	$0.17 \pm 0.11$	$0.27 \pm 0.02$	$0.22 \pm 0.10$	$0.98 \pm 0.01$	19.221	0.006
054-31132	11.0230636	41.6583295	5.9	$\leq 0.26$	$0.39 \pm 0.04$	$0.21 \pm 0.10$	$0.95 \pm 0.05$	20.417	-0.159
054-44407	11.3321220	41.7514398	8.1	$0.29 \pm 0.24$	$0.23 \pm 0.03$	$0.16 \pm 0.04$	$0.99 \pm 0.01$	19.605	-0.187
055-01161	10.5500807	41.4274429	8.9	$0.28 \pm 0.06$	$0.32 \pm 0.05$	$0.17 \pm 0.06$	$0.98 \pm 0.03$	19.134	0.139
055-19435	10.7472466	41.6185303	14.0	$0.18 \pm 0.05$	$0.16 \pm 0.03$	$0.08 \pm 0.03$	$1.00 \pm 0.01$	20.450	0.342
055-20813	10.7648537	41.6311487	11.0	$\leq 0.14$	$0.26 \pm 0.03$	$0.11 \pm 0.03$	$1.00 \pm 0.02$	20.498	0.372
063-35392	11.5440668	42.2123537	2.4	$\leq 0.29$	$0.28 \pm 0.01$	$0.08 \pm 0.03$	$1.00 \pm 0.05$	19.618	-0.148



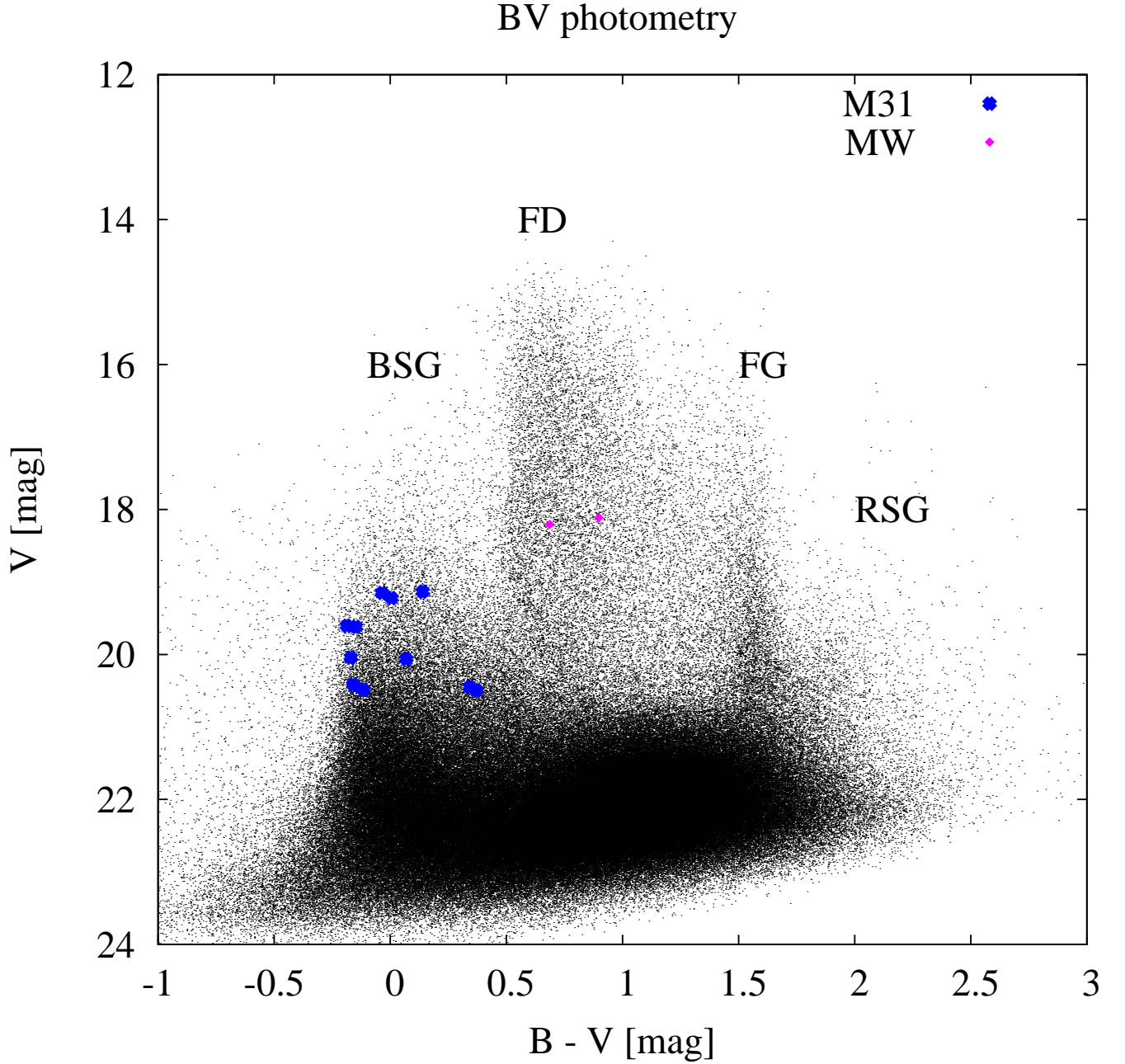


Fig. 7.— Color magnitude diagram for the 13 bright detached binaries. The underlying black dots are photometric measurements taken from the Local Group Galaxy Survey (Massey et al. 2006). Different M31 and Milky Way populations are clearly separated, e.g. blue super giants (BSG) and red super giants (RSG) in M31, foreground dwarves (FD) and foreground giants (FG) from Milky Way. The two brightest detached binaries (marked in pink rhombi) from our sample exhibit relative red color, fit into the foreground dwarf scenario, while the remaining 11 systems (marked in blue dots) are bluer, and better fit into the M31 blue giants scenario.

## 6. Summary

We have established a customized pipeline that generates difference imaging light-curves for the PS1 M31 data. Possible variable candidates are selected with a simple  $\chi^2$  criterion. We apply a modified box-fitting algorithm to determine their period and identify eclipsing binary candidates. These candidates are further classified into categories of detached, semi-detached, and contact systems with Fourier decomposition, which is carried out for M31 binaries for the first time. The period distribution shows detached and semi-detached systems are longer, peaked at  $> 10$  days, while the contact systems have rather short periods. The only exception is a contact system with period larger than 10 days. Such a system can be explained by a semi-detached configuration, where one of the component is Roche-lobe filling, while the other component is considerably smaller or cooler. The red color of this systems indeed points towards the semi-detached scheme.

Following the classification, we cross-match our detached binaries with the Local Group Galaxy Survey, and select 13 systems brighter than 20.5 mag in V, rendering its spectroscopic follow-up with 8-10m class ground-based telescopes feasible. We note that the distance to M31 has been determined to  $\sim 4\%$  accuracy using two binary systems (Vilardell et al. 2010). However, these two binaries are semi-detached, which complicate the light curve analysis with distortions and reflection effects due to proximity of the components. In our detached binary sample, there are several systems exhibit eccentric orbits, where the components can be considered well separated, and reduce the complexity of light curve modelling.

## 7. Acknowledgments

We would like to thank the referee for the insightful comments. This work was supported by the DFG cluster of excellence 'Origin and Structure of the Universe' ([www.universe-cluster.de](http://www.universe-cluster.de)) and its Munich Institute for Astro and Particle Physics (MIAPP, [www.munich-iapp.de](http://www.munich-iapp.de)). RPK acknowledges support by the National Science Foundation under grant AST-1008798. The Pan-STARRS1 Surveys (PS1) have been made possible through contributions of the Institute for Astronomy, the University of Hawaii, the Pan-STARRS Project Office, the Max-Planck Society and its participating institutes, the Max Planck Institute for Astronomy, Heidelberg and the Max Planck Institute for Extraterrestrial Physics, Garching, The Johns Hopkins University, Durham University, the University of Edinburgh, Queen's University Belfast, the Harvard-Smithsonian Center for Astrophysics, the Las Cumbres Observatory Global Telescope Network Incorporated, the National Central University of Taiwan, the Space Telescope Science Institute, the National Aeronautics and Space Administration under Grant No. NNX08AR22G issued through the Planetary Science Division of the NASA Science Mission Directorate, the National Science Foundation under Grant No. AST-1238877, the University of Maryland, and Eotvos Lorand University (ELTE).

## REFERENCES

- Alard C., Lupton R. H., 1998, *ApJ*, 503, 325
- Bonanos, A. Z., Stanek, K. Z., Sasselov, D. D., et al. 2003, *AJ*, 126, 175
- Bonanos, A. Z., Stanek, K. Z., Kudritzki, R. P., et al. 2006, *ApJ*, 652, 313
- Clementini, G., Federici, L., Corsi, C., et al. 2001, *ApJ*, 559, L109
- Derekas, A., Kiss, L. L., & Bedding, T. R. 2007, *ApJ*, 663, 249
- Devor, J. 2005, *ApJ*, 628, 411
- Freedman, W. L., Madore, B. F., Gibson, B. K., et al. 2001, *ApJ*, 553, 47
- Gil de Paz A., et al., 2007, *ApJS*, 173, 185
- Kaluzny, J., Stanek, K. Z., Krockenberger, M., et al. 1998, *AJ*, 115, 1016
- Kaluzny, J., Mochejska, B. J., Stanek, K. Z., et al. 1999, *AJ*, 118, 346
- Kodric, M., Riffeser, A., Hopp, U., et al. 2013, *AJ*, 145, 106
- Koppenhoefer, J., Saglia, R. P., & Riffeser, A. 2013, *Experimental Astronomy*, 35, 329
- Kovács, G., Zucker, S., & Mazeh, T. 2002, *A&A*, 391, 369
- Lee, C.-H., Riffeser, A., Koppenhoefer, J., et al. 2012, *AJ*, 143, 89
- Lee, C.-H., Kodric, M., Seitz, S., et al. 2013, *ApJ*, 777, 35
- Macri, L. M. 2004, *IAU Colloq. 193: Variable Stars in the Local Group*, 310, 33
- Magnier E., 2006, *amos.conf*,
- Magnier, E. A., Liu, M., Monet, D. G., & Chambers, K. C. 2008, *IAU Symposium*, 248, 553
- Massey P., Olsen K. A. G., Hodge P. W., Strong S. B., Jacoby G. H., Schlingman W., Smith R. C., 2006, *AJ*, 131, 2478
- Mochejska, B. J., Kaluzny, J., Stanek, K. Z., Krockenberger, M., & Sasselov, D. D. 1999, *AJ*, 118, 2211
- Nefs, S. V., Birkby, J. L., Snellen, I. A. G., et al. 2012, *MNRAS*, 425, 950
- Paczyński, B. 1997, *The Extragalactic Distance Scale*, 273
- Paczyński, B., Szczygieł, D. M., Pilecki, B., & Pojmański, G. 2006, *MNRAS*, 368, 1311

- Pojmanski, G. 2002, *Acta Astron.*, 52, 397
- Ribas, I., Jordi, C., Vilardell, F., et al. 2005, *ApJ*, 635, L37
- Rucinski, S. M. 1993, *PASP*, 105, 1433
- Rucinski, S. M. 1996, *The Origins, Evolution, and Destinies of Binary Stars in Clusters*, 90, 270
- Rucinski, S. M., & Maceroni, C. 2001, *AJ*, 121, 254
- Samus, N. N., Durlevich, O. V., & et al. 2009, *VizieR Online Data Catalog*, 1, 2025
- Stanek, K. Z., Kaluzny, J., Krockenberger, M., et al. 1998, *AJ*, 115, 1894
- Stanek, K. Z., Kaluzny, J., Krockenberger, M., et al. 1999, *AJ*, 117, 2810
- Vilardell, F., Ribas, I., & Jordi, C. 2006, *A&A*, 459, 321
- Vilardell, F., Ribas, I., Jordi, C., Fitzpatrick, E. L., & Guinan, E. F. 2010, *A&A*, 509, A70
- Wyithe, J. S. B., & Wilson, R. E. 2002, *ApJ*, 571, 293
- Zendejas Dominguez, J., Koppenhoefer, J., Saglia, R. P., et al. 2013, *A&A*, 560, A92